Capacity Usage Determination of a Capacitor-less D-STATCOM considering Power System Uncertainties

Aaqib Peerzada
Texas A&M University
College Station, TX

Miroslav Begovic
Texas A&M University
College Station, TX

Wesam Rohouma
University of North Atlantic
Doha, Qatar

Robert S. Balog
Texas A&M University
College Station,TX

Abstract

The increasing adoption of distributed energy resources (DERs), particularly solar generation and the use of unconventional loads such as plug-in electric vehicles (PHEVs), has a profound impact on the planning and operation of electric distribution systems. In particular, PHEV charging introduces stochastic peaks in energy consumption, while solar generation is fraught with variability during intermittent clouds. The stochastic nature of such DERs renders the operation of mechanical assets such as on-load tap changers and switched capacitor banks ineffective. A possible solution to mitigate the undesirable effects of DERs is using solid-state-based devices such as a distribution static synchronous compensator (D-STATCOM). This paper examines the capacity usage of a capacitor-less D-STATCOM in distribution systems while considering the uncertainties associated with using the aforementioned DERs. We propose a Monte Carlo simulation to study the capacity usage problem with DER inputs sampled from the proposed underlying distributions.

1. Introduction

In electric distribution systems, reactive power compensation in the form of voltage regulation and power factor correction is typically realized using electromechanical assets such as on-load tap changers (OLTCs) and switched capacitor banks (SCBs). However, given the mechanical nature of the operation, such legacy devices are not suitable for providing reactive power compensation at shorter time scales of minutes or seconds. The output of a PV system is a function of weather primarily at a given location and can experience rapid changes that necessitate a continuously adjustable reactive power compensation for precise voltage control. One class of devices capable of providing dynamic voltage control is the smart PV inverters. However, the PV inverters are limited in providing continuous reactive support constrained by the inverter's apparent power sizing [1]. The PV inverters are also not owned by the utility and, in most situations, do not respond to the dispatch commands issued by the network operator [2].

Other examples of power electronics-based solid-state devices used for mitigating the adverse impact of DERs include static var compensators (SVCs) at transmission or sub-transmission voltage levels and D-STATCOMs based on voltage source converter (VSC) technology. A major disadvantage of the SVCs is the lack of harmonic control functionality and exorbitant capital costs in low voltage regimes [3]. Due to these reasons, SVCs are inherently not suitable for use in low-voltage networks that are plagued by power quality issues due to the increased use of nonlinear loads. On the other hand, the VSC-based D-STATCOMs rely on electrolytic capacitors (E-caps) for energy storage. The reliance on E-caps adversely affects the reliability of the VSC-based D-STATCOMs, especially in locations with tropical climate conditions [3]. The literature on the reliability of the power electronics devices has established that nearly 30% of all the failures in power electronics-based devices are caused by the E-caps [2].

In the light of these observations, a capacitor-less D-STATCOM based on a matrix converter (MC) has been proposed recently to address the dual challenges of fast reactive support and increased reliability [4]. The newly proposed capacitor-less D-STATCOM uses inductive storage and is controlled using a finite control set model predictive control (MPC). The capacitor-less D-STATCOM is a multi-functional device that can be used for power factor correction, voltage regulation, and harmonic compensation simultaneously with local autonomous control or directly controlled by the distribution network operator (DSO). A comparison between the capacitor-less MC-based D-STATCOM and the incumbent technologies is given in [3]

Uncertainty quantification (UQ) in power networks, especially distribution systems, is an emerging area of research that has attracted much attention from the

URI: https://hdl.handle.net/10125/102950
978-0-9981331-6-4

power system research community. The increased popularity of UQ methods to combat uncertainty challenges can be attributed to the rise of DERs, especially intermittent nonscheduled generation like solar and wind, and more recently, the accelerated growth of PHEVs. To the best of our knowledge, the current literature on the stochastic modeling of electric vehicle charging is scarce and limited to models based on queuing theory. The electric vehicle charging as a queuing process is studied in [5], [6], [7]. A significant drawback of the proposed methods is the lack of information on the simulation of the arrival times of the PHEVs. Most of the proposed models rely on either real-time sub-metering data [6] or the intensity functions based on measured arrival rates of the vehicles queuing up to receive charging service [5]. In this paper, we use a stochastic counting process based on a nonhomogeneous Poisson process (NHPP) to simulate the arrival times of the PHEVs. The information about the arrival times is necessary to model the temporal dependence of the PHEV charging accurately.

An undesirable effect of PHEV charging is the "peaky" energy consumption patterns that, in the absence of proper modeling and mitigation, could lead to thermal overloading of transformers and transmission lines. In this paper, we use a mixture model based on generalized Gaussian distribution to model the statistical uncertainty of DER-impacted load. A generalized Gaussian distribution represents an improvement over the conventionally used mixture model based on Gaussian distribution [8]. The improvement is a result of additional parameters that control the shape of the fitting distribution. The power system load is also affected by the penetration level and the configuration of the distributed generation. In the case of distributed rooftop solar generation, the effect is more pronounced when the output of a photovoltaic (PV) system is viewed at sub-hourly or sub-minute time scales [9]. It is thus essential to accurately model the sub-hourly changes in the solar output to properly assess the impact on the local load at a load bus and the diversified demand as seen from the secondary of the distribution substation transformer. The Markov weather model proposed in [9] is used to create a high resolution (1-minute) solar irradiance profile based on the hourly averaged Typical Meteorological Data (TMY3) [10]. The solar forecast scenarios for the proposed Monte Carlo simulation are developed using an auto-regressive moving average (ARMA) model. Statistical models such as ARMA have been widely used to generate solar power scenarios despite the inherent limitations of these models [11]. One such limitation is the need for large data sets to train the model. In this paper, we use the annual synthetic high-resolution data from the Markov weather model to estimate the ARMA model's orders and parameters. The fully realized ARMA model is used to generate solar power scenarios.

A major significance of this paper is that it studies the interaction of a power electronics converter in terms of its capacity usage when integrated with an electric distribution system without neglecting the details of either. A complete model of the IEEE-34 bus distribution test system [12] is developed in OpenDSS [13]. The steady-state power system models of the capacitor-less D-STATCOM in different modes of operation are developed in a MATLAB environment and interfaced with the OpenDSS solver. It is important to emphasize that while the focus of this paper is to develop a probabilistic capacity usage model of the capacitor-less D-STATCOM, a rigorous treatment of the computational methods used for uncertainty quantification of the inputs of the Monte Carlo simulation, which in this case are bus load, PHEV charging, and rooftop solar generation, is crucial to answering the central question.

2. Capacitor-less D-STATCOM

The capacitor-less D-STATCOM performs the same functions as the existing VSC-based D-STATCOM. A distinction, however, can be drawn in terms of the circuit elements used for energy storage. The capacitor-less D-STATCOM uses inductors for energy storage as opposed to electrolytic capacitors. This enables the capacitor-less D-STATCOM to achieve a much longer service life, especially in regions with harsh climatic conditions [2]. The capacitor-less D-STATCOM is designed to provide reactive power compensation to simultaneously address the multiple challenges of power factor correction, voltage regulation, and harmonic mitigation. The proposed converter can work either in a local autonomous mode and determine the amount of reactive power to be injected or absorbed or can be centrally dispatched by the system operator. This multiplicity of operation is a benefit that a utility can derive from the converter, and the resulting monetary savings can offset the high capital cost of the device for use in low-voltage distribution systems.

2.1. Converter Topology

The three phase matrix converter (MC) with nine bidirectional switches, three phase input filter and output chokes is the fundamental building block of the proposed converter. The bidirectional switches are realized by means of two anti-parallel IGBT-diode pairs for bidirectional flow. The shunt-connected MC-based

capacitor-less D-STATCOM is shown in Figure 1 . The

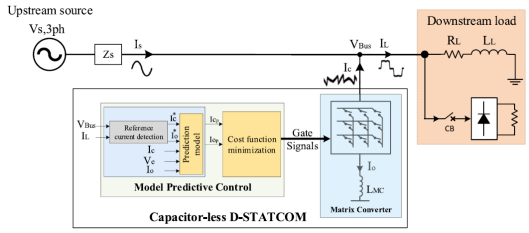

Figure 1. Matrix Converter-based capacitor-less D-STATCOM [3]

converter design uses Model Predictive Control (MPC) strategy to achieve phase current inversion between the input and output currents. The input and output current relations of the MC are given in (1)

$$\begin{bmatrix} I_{cA} \\ I_{cB} \\ I_{cC} \end{bmatrix} = \begin{bmatrix} S_{Aa} & S_{Ab} & S_{Ac} \\ S_{Ba} & S_{Bb} & S_{Bc} \\ S_{Ca} & S_{Cb} & S_{Cc} \end{bmatrix} \begin{bmatrix} I_{0A} \\ I_{0B} \\ I_{0C} \end{bmatrix} \quad (1)$$

The input and output voltages share the same relationship. The switching function S_{ij} can be either 0 or 1, where $i \in [A, B, C]$ and $j \in [a, b, c]$. The phase reversals are achieved by making good choices about S_{ij} which makes inductive energy storage appear capacitive at the input of the MC. More details on the MC are given in [4].

2.2. Power Factor Correction Operation

In OpenDSS the capacitor-less D-STATCOM in power factor correction mode is modeled as an ideal current source and the compensating currents and the reactive powers for each phase of the load are calculated based on phase admittance and the phase voltage. In general a three phase load with phase A admittance $Y_A = G_A + jB_A$, and phase voltage $\overline{V}_A$the phase current is

$$\overline{I}_A = \overline{V}_A Y_A = V_A \angle\theta_A (G_A + jB_A) = I_{RA} + jI_{XA} \quad (2)$$

The capacitor-less D-STATCOM as an ideal current source is shunt connected to compensate for the phase quadrature component I_{XA} of the phase A load current. If the phase A compensating current is I_{CA} and $I_{CA} = -I_{XA}$ the phase A converter rating is

$$S^{pf}_{CA} = \overline{V}_A \overline{I}^*_{CA} = \overline{V}_A(-j\overline{V}_A B_A) = j\overline{V}^2_A B_A \quad (3)$$

Equation (3) suggests that only the reactive power demand of phase A of the load is compensated while the real power demand remains unaffected. Since the reactive power demand of phase A of the load is $Q_A = -\overline{V}^2_A B_A$, the converter rating can be expressed solely in terms of Q_A.

$$S^{pf}_{CA} = -jQ_A = jQ^{pf}_{CA} \quad (4)$$

From (4) we can conclude that if the compensator, the ideal current source modeling the steady state behavior of the the capacitor-less D-STATCOM in this case, is desired to provide power factor correction, the condition for unity power factor operation of phase A of the load is $Q^{pf}_{CA} = -Q_A$. Partial compensation can be achieved if $|Q^{pf}_{CA}| = \alpha|Q_A|, 0 < \alpha < 1$. The phasor compensating current required to achieve full compensation (unity power factor) of Phase A is

$$\overline{I}_{CA} = \frac{S^{pf}_{CA}}{\overline{V}^*_A} = \frac{-jQ^{pf}_{CA}}{\overline{V}^*_A} = \frac{-j\left(S_A\sqrt{1-\cos^2\phi_A}\right)}{\overline{V}^*_A} \quad (5)$$

In (5) Q^{pf}_{CA} is the reactive power rating of the converter, S_A is the apparent power of phase A of the load and $\cos\phi_A$ is the phase A power factor. The compensatory ideal current source model of (2-5) is implemented in MATLAB environment and interfaced with OpenDSS solver engine via the Component Object Model (COM) interface. The compensating currents for each phase of the load are updated after successful convergence of the power flow and injected into the load. The total three phase reactive power rating of the converter in power factor correction mode is the sum of reactive power ratings for each phase. That is $Q^{pf}_{3\phi} = Q^{pf}_{CA} + Q^{pf}_{CB} + Q^{pf}_{CC}$.

2.3. Voltage Regulation Operation

The power system steady state model of the capacitor-less D-STATCOM in voltage regulation mode is based on the reactive power mismatch equations. A proportional-integral controller is used to minimize the mismatch between the reference voltage (voltage set-point) and the measured bus voltage. The first two equations model the reactive power exchange between the converter and the load bus and the third equation models the control scheme .

$$0 = \begin{bmatrix} Q^{vr}_{3\phi} - V_L I_{line}\sin(\theta_{V_L} - \theta_{I_{line})} \\ Q^{vr}_{3\phi} + |V_L|^2 B_l - |V'|G_l \sin\delta + |V'|B_l\cos\delta \\ V_L - V_{sp} \end{bmatrix} \quad (6)$$

In (6) $Q^{vr}_{3\phi}$ is the total three phase reactive power exchanged between the converter and the load bus, B_l and G_l are the line susceptance and conductance respectively connecting the converter and the bus, V_L, θ_{V_L} is the bus voltage magnitude and angle

respectively,I_{line}, $\theta_{I_{line}}$ are the line current magnitude and angle respectively, $|V'| = |V_L||V_{conv}|$, V_{conv} is the converter voltage magnitude, $\delta = \theta_{V_L} - \theta_{V_{conv}}$, $\theta_{V_{conv}}$ is the converter voltage angle and V_{sp} is the voltage set-point of the converter.

3. Design of Uncertainty

The probabilistic capacity usage model of the capacitor-less D-STATCOM is developed by Monte Carlo sampling of the input variables. For a given penetration level of the solar generation, the input variables of the Monte Carlo simulation are the bus load profile, PHEV charging profile, and PV generation profile. The use of Monte Carlo sampling entails that the capacity usage Q be a random variable that can assume a range of values. When the random variable Q is indexed by time, it represents a stochastic process $\{Q_t; 0 \leq t < \infty\}$ defined on the probability space Ω_Q. The stochastic process Q_t is continuous and its distribution is described by the probability density $f_{Q_t}(q,t)$. The density function $f_{Q_t}(q,t)$ describes the joint distribution of the random variables $\{Q_t; 0 \leq t < \infty\}$. The Monte Carlo simulation estimates the expectation of any Borel-measurable function $h : \mathbb{R} \longrightarrow \mathbb{R}$ of the stochastic process Q_t.

$$\mathbf{E}[h(Q_t)] = \int_{q\in\Omega_Q} h(Q_t) f_{Q_t}(q,t) dq \tag{7}$$

The Monte Carlo estimator of (7) can be obtained by running Monte Carlo simulations with inputs sampled from the underlying distributions. The inputs considered for the estimation of (7) are the PHEV charging, load profile and the solar generation profile.

3.1. PHEV Charging Scenarios

The stochastic PHEV charging scenarios are developed by considering a stochastic counting process $\{N_{EV}(t); t \geq 0\}$ defined on the probability space Ω_{EV}. The random variable $N_{EV}(t)$ is the realization of the number of PHEV arrivals in the interval $[0,t]$. The counting process considered has the property $N_{EV}(\tau) \geq N_{EV}(t)$ for any $\tau \geq t$. This implies that the random variable $N_{EV}(\tau) - N_{EV}(t)$ is nonnegative. By the virtue of this definition, the counting process $\{N_{EV}(t); t \geq 0\}$ is integer valued, nondecreasing and right continuous consistent with the real world physics of the PHEV arrivals at a charging station. Furthermore, to be consistent with the real world rate of arrival of PHEVs at a charging location, we consider the stochastic counting process $\{N_{EV}(t); t \geq 0\}$ to be a nonhomogeneous Poisson process (NHPP) with a time-varying arrival rate $\lambda(t)$ such that $\forall t \geq 0$ and $\delta > 0$ satisfies

$$\begin{aligned}
&\Pr\{\tilde{N}_{EV}(t, t+\delta) = 0\} = 1 - \lambda(t)\delta + o(\delta^2) \\
&\Pr\{\tilde{N}_{EV}(t, t+\delta) = 1\} = \lambda(t)\delta + o(\delta^2) \\
&\Pr\{\tilde{N}_{EV}(t, t+\delta) \geq 2\} = o(\delta^2)
\end{aligned} \tag{8}$$

In (8) $\tilde{N}_{EV}(t, t+\delta) = N_{EV}(t+\delta) - N_{EV}(t)$. The NHPP defined in (8) has the independent increment property but lacks the stationary increment property. The NHPP in (8) is characterized by a mean value function $\wedge(t) = \mathbf{E}[N_{EV}(t)] = \int_0^t \lambda(y)dy < \infty$. The probability of r arrivals in the interval $[0,t]$ is

$$\Pr\{N_{EV}(t) - N_{EV}(0) = r\} = \frac{[\wedge(t) - \wedge(0)]^r}{r!} \exp(-[\wedge(t) - \wedge(0)]) \tag{9}$$

Unlike a homogeneous Poisson process (HPP), the interarrival times of a NHPP are neither independent nor exponentially distributed. More specifically, the cdf of the r^{th} interarrival time $X_r = S_{r+1} - S_r$ conditioned on the first r arrival times $S_1 = s_1, S_2 = s_2, ..., S_r = s_r$ is

$$F_{X_r}(x) = \Pr\{X_r \leq x | S_i = s_i, i = 1, 2, ..., r\} \tag{10}$$

The conditional cdf in (10) can also be written in terms of number of arrivals in the interval $N(S_r + x) - N(S_r)$ conditioned on the r^{th} arrival.

$$F_{X_r}(x) = \Pr\{N(S_r + x) - N(S_r) \geq 1 \mid S_r = \textstyle\sum_{i=1}^{r} X_i\} \tag{11}$$

The arrival times of a NHPP can be simulated from a HPP by considering a constant rate function λ^+ that dominates the time-varying rate function $\lambda(t)$ of the desired NHPP such that $\lambda^+ \geq \lambda(t) \forall t \in [0,T]$. The "thinning" algorithm is used to sample from the generated events of a HPP such that the desired rate function $\lambda(t)$ is achieved. It is a variation of "acceptance-rejection" algorithm and is based on the theorem of Lewis and Shedler, 1979 [14]. The proof is given in [15]. In this work we consider a piecewise constant arrival rate function in 30 minute intervals. The piecewise constant arrival rate function is based on the real-world data given in [5]. The thinning algorithm is applied to the data to generate the arrival times that are consistent with the real-world arrival of PHEVs at a charging station. The generated scenarios of the counting process $\{N_{EV}(t)\}$ as a function of the arrival times S_r based on the real-world arrival rate are shown in Fig . The output of the thinning algorithm is used to construct the PHEV charging scenarios based on the procedure presented in [16] .

Algorithm 1: Acceptance Rejection based Thinning of HPP

Input:NHPP Intensity function $\lambda(t)$, HPP Constant-rate Intensity function λ^+, Interval length $[0, T]$)
Set $\lambda^+ = \max\{\lambda(t)\}$
Set the counting process $N_{EV} = a\lambda^+ T, a > 1$
while $i \leq N_{EV}$ **do**
  Draw $u \sim U(0, 1)$
  Set $S_r = -\frac{1}{\lambda^+} \log u_r$
end while
Set $\mathbf{S} = \mathbf{S}(\mathbf{S} < N_{EV})$
Set $r^* = \max\{r; \sum_{n=1}^{r} S_n < T\}$
for all i=1,..,r **do**
  Draw $w \sim U(0, 1)$
  Calculate acceptance probability, $r(j) = \frac{\lambda(S_j)}{\lambda^+}$
  if $w_j \leq r(j)$ **then**
    $\mathbf{I}_j = 1$
  else
    $\mathbf{I}_j = 0$
  end if
end for
$\mathbf{J} = \{\mathbf{I}_j; j = 1\}$
$S_j^{NHPP} = \{S_j; j \in \mathbf{J}\}$
Output: Arrival Times of NHPP

3.2. Annualized Load Scenarios

To generate the load scenarios with similar statistical properties as the measured load data we propose using a probability mixture model based on a generalized Gaussian distribution. The proposed mixture model is "generative" and can be used to sample random numbers from the empirical statistical distribution of the load. A probability mixture model is a convex combination of a finite number of probability densities with associated nonnegative weights. This property lends a mixture model well suited for fitting probability densities with multi-modal characteristics. In general, a mixture model that is a sum of a finite number of density functions has the following form

$$f_Y(y_i; \Psi) = \sum_{j=1}^{M} \pi_j p_{j,Y}(y_i, C = j, \Theta_j) \qquad (12)$$

In the context of load modeling, $Y = y_i$ is the measured load data, M is the number of mixture components and $\pi_j = p(y_i \in C_j)$ is the weight of the j^{th} component density. The weights assigned to component densities are subject to $\pi_j > 0 \ \forall j \in \{1, 2, ..., M\}$ and $\sum_{j=1}^{M} \pi_j = 1$. The component density $p_{j,Y}$ is parameterized by Θ_j and $\Psi = \{\pi_j, \Theta_j; j = [1, 2, ..., M]\}$ is the overall parameter vector. Estimating Ψ in a mixture model is quite challenging since the optimization of the log-likelihood of $f_Y(y_i; \Psi)$ is often ill-posed. The log-likelihood function of (12) has the form

$$\log L(\Psi|y_i) = \sum_{i=1}^{N} \log \sum_{j=1}^{M} \pi_j p_{j,Y}(y_i|C = j, \Theta_j) \quad (13)$$

The maximization of (13) cannot be done using the maximum-likelihood method (MLE) because of the $\log(\sum)$ term. A solution to the maximization of (13) is possible however using the Expectation-Maximization algorithm (E-M) [17]. The E-M algorithm find a solution by reinterpreting the measured data Y as incomplete data and posits the existence of a $M-$ dimensional binary variable $\mathbf{Z} = \{z_{ji}\}_{i=j=1}^{i=N,j=M}$ for each sample y_i such that the j^{th} component z_{ji} is 1 if and only if y_i belongs to the j^{th} component. That is

$$z_{ji} = \begin{cases} 1, y_i \in C_j \\ 0; y_i \notin C_j \end{cases} \qquad (14)$$

To capture the statistical properties of the measured load data Y with high accuracy we propose using generalized Gaussian distributions as component densities for the mixture model in (12). A random variable Y has a generalized Gaussian distribution if the density function of Y has the form

$$p_Y(y; \mu, s, p) = \frac{\beta}{2s\Gamma\left(\frac{1}{\beta}\right)} \exp\left[-\frac{|y - \mu|^\beta}{s^\beta}\right] \qquad (15)$$

In 15, $\beta \in \mathbb{R}^+$ is the shape parameter,$s \in \mathbb{R}^+$ is the scale parameter, $\mu \in \mathbb{R}$ is the location parameter and $\Gamma(.)$ is the gamma function. It is worth noting that $\beta = 1$ gives a Laplace distribution and $\beta = 2$ gives a Gaussian distribution. The generalized Gaussian distribution is more flexible than a Gaussian distribution. The increased flexibility is due to the extra shape parameter β which can be optimized to represent a large variety of statistical behaviors. This is important in the context of statistical load modeling since this means that a generalized Gaussian distribution can approximate the peak load behavior better than a Gaussian distribution.

For a mixture model with component densities given in (15), the application of E-M algorithm results in the following update equations for the overall parameter vector $\Psi^{(n+1)} = \{\pi_j, \mu_j, s_j, \beta_j; j = [1, 2, ..., M]\}$ given the current estimate Ψ^n and the measured load data Y

$$\pi_j^{(n+1)} = \frac{1}{N} \sum_{i=1}^{N} \mathbf{E}\left[z_{ji}|Y, \Psi^{(n)}\right] \qquad (16)$$

$$\sum_{i=1}^{N} \mathbf{E}\left[z_{ji}|Y,\Psi^{(n)}\right]\beta_j^{(n)}|\mu_j^{(n+1)}-y_i|^{\beta_j^{(n)}}=0 \quad (17)$$

$$s_j^{(n+1)}=\left[\frac{\sum_{i=1}^{N}\mathbf{E}\left[z_{ji}|Y,\Psi^{(n)}\right]}{\sum_{i=1}^{N}\mathbf{E}\left[z_{ji}|Y,\Psi^{(n)}\right]\beta_j^{(n)}|\mu_j^{(n+1)}-y_i|^{\beta_j^{(n)}}}\right]^{-\frac{1}{\beta_j^{(n)}}} \quad (18)$$

$$\sum_{i=1}^{N}\mathbf{E}\left[z_{ji}|Y,\Psi^{(n)}\right]\kappa=0 \quad (19)$$

In (19), κ equals

$$\kappa=\frac{1}{\beta_j^{(n+1)}}+\frac{\psi\left(1/\beta_j^{(n+1)}\right)}{\left(\beta_j^{(n+1)}\right)^2}-\left(\frac{|y_i-\mu_j^{(n)}|}{s_j^{(n)}}\right)^{\beta_j^{(n+1)}}\left(\log|y_i-\mu_j^{(n)}|-\log s_j^{(n)}\right) \quad (20)$$

In (20) $\psi(.)$ is the digamma function defined as $\Gamma'(h)/\Gamma(h)$. The update equations for the μ and β are nonlinear and we use the Newton-Raphson method to obtain a numerical solution.

3.3. Distributed Generation Scenarios

The Markov weather model proposed in [9] can generate high-resolution solar irradiance data with high enough fidelity to reproduce the rapid excursions in the output of a solitary PV system. The estimation of the clearness index, which is defined as the ratio of measured irradiance at the earth's surface at a location and the cloudless sky irradiance at the same location, is central to the Markov weather model. The Markov weather model works by combining the low-resolution clearness index based on the hourly averaged TMY3 [10] data with transition probabilities generated at sub-hourly time scales from measured high-resolution data. This results in an output with a high temporal resolution, 1-minute in this case, and seasonal variation.

The solar output of a PV system can be modeled as a continuous stochastic process. Since optimization of continuous stochastic processes is complicated and even impossible in many cases, a discrete-time approximation is often used in formulating optimization problems. The continuous stochastic process G_{PV}^i representing power generated at bus i in a network can be well approximated by a discrete process $\hat{G}_{PV}^i$ such that

$$\hat{G}_{PV}^i=\{\hat{G}_{PV}^i(t,\omega)=[g_{PV}^i(1,\omega),g_{PV}^i(2,\omega),...,g_{PV}^i(T,\omega)],\omega=1,2,...,H\} \quad (21)$$

In (21) T is the length of the time horizon, ω is the scenario index, and H is the number of possible scenarios, which is also equal to the number of Monte Carlo runs. The stochastic process $\hat{G}_{PV}^i$ is completely determined by the joint distribution of the random variables $\{g_{PV}^i(t,\omega);t=1,2,...,T,\omega=1,2,...,H\}$. The joint distribution can also be used to evaluate the marginal distribution of the random variable $g_{PV}(t,\omega)$ and the statistical dependencies that exist among these random variables. The estimation of the joint distribution, however, is challenging and is simplified by assuming that the joint distribution is a multivariate Gaussian and the stochastic process $\hat{G}_{PV}^i$ is stationary. The assumption of a multivariate Gaussian implies that the marginal distributions are all univariate Gaussian. The assumption of stationarity implies that the mean, variance, and covariance of the stochastic process $\hat{G}_{PV}^i$ are time-invariant. .

With these assumptions the joint distribution of the stochastic process $\hat{G}_{PV}^i$ can be determined by ARMA modeling of the time series data. The time series data used to train the ARMA model is obtained from the Markov weather model. Mathematically, an ARMA (p,q) model with p auto-regressive parameters and q moving average parameters has the form

$$g_{PV}^i(t,\omega)=\sum_{i=1}^{p}\phi_i g_{PV}(t-i,\omega)+\epsilon(t)+\sum_{j=1}^{q}\theta_j\epsilon(t-j) \quad (22)$$

In (22) the term $\epsilon(t)$ is an uncorrelated stochastic process with zero mean and variance σ_ϵ^2. The stochastic process $\epsilon(t)$ is called white noise or innovation term. Before realizing the ARMA (p,q) model, i.e., estimating the model orders and coefficients, it is important to test whether the stationarity assumption holds for the time series data used to train the ARMA model in (22). The annual 1-minute time series data from the Markov weather model is tested for stationarity using the Augmented Dickey-Fuller (ADF) test [18]. The ADF test contains the null hypothesis that the time series is non-stationary. The test result rejects the null hypothesis, implying that the series may be stationary and that the use of the ARMA model may be justified.

The ARMA model orders p,q and the model coefficients $\phi_1,...,\phi_p$ and $\theta_1,...,\theta_q$ are estimated by implementing the model in the System Identification Toolbox (SIM) in MATLAB [19]. Using the high-resolution time series solar generation data from the Markov weather model, the SIM constructs mathematical models with different combinations of model orders. The order combination with the least Bayesian Information Criterion (BIC) value is selected. Conversely, the order combination with the largest log-likelihood value is chosen since large log-likelihood values represent better fits.

4. Results and Discussion

This section will present the results of the scenario generation algorithms for PHEV charging, statistical load distributions, and distributed generation. The scenarios thus generated for each of the inputs are used to run the Monte Carlo simulations, and the capacity usage of the capacitor-less D-STATCOM is studied based on (5) and (6). To assess the capacity usage of the converter over a wide range of operational conditions, we design annual Monte Carlo simulations with a random sampling of the inputs from annualized scenarios. The step size of the power flow simulations is 1-minute. The simulations were performed on a fully detailed model of the IEEE-34 bus distribution test feeder implemented in OpenDSS. The capacitor-less D-STATCOM is assumed to be connected at Bus 890 of the test feeder. The D-STATCOM location is chosen based on the base voltage profile of the feeder under peak load conditions [4]. Fig 2 shows the one-line diagram of the IEEE 34 bus feeder with the proposed converter shunt connected at bus 890 to provide reactive power compensation. The PHEV charging scenarios

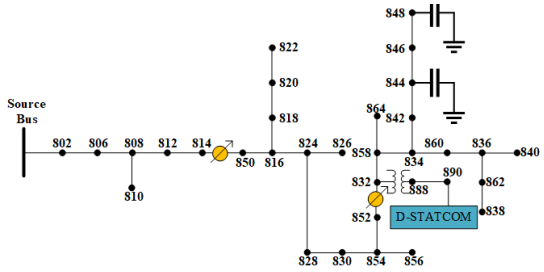

Figure 2. IEEE 34 Bus Test Feeder with Shunt Connected D-STATCOM

are developed based on the PHEV arrival scenarios using the procedure outlined in [16]. Each charging scenario is developed based on the expectation of the corresponding counting process $\{N_{EV}(t); t > 0\}$, the energy required to charge the PHEVs, and the charging time. The energy required to charge a PHEV depends on the initial and final state of charge (SoC). The initial SoC or the SoC at the arrival depends on the vehicle's energy consumption in $100kWh/100$ miles, daily driven miles, and the battery capacity. We assume a fleet of Tesla Model 3 and three-phase level 2 (L-2) charging. The thinning algorithm described earlier is applied to the piecewise constant arrival rate of the PHEVs queuing up at a charging station to receive a charging service. The piecewise constant arrival rate data is given in [5]. Figure 3 shows hundred example scenarios of the stochastic counting process $N_{EV}(t)$ for one day. The generalized Gaussian mixture model described earlier is

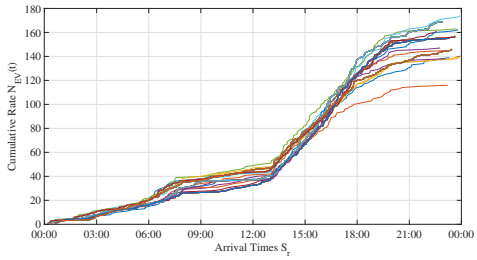

Figure 3. PHEV Cumulative Arrival Scenarios

used to generate load scenarios with similar statistical properties as the measured (empirical) load data. Bus 890 of the test feeder is assumed to be a commercial load. This assumption is based on the peak active and reactive load ratings provided in the original feeder data developed by the IEEE distribution subcommittee. The measured historical annual commercial load profile (without PHEV charging) is obtained from the OpenEI website [20]. The web page is sponsored by the U.S Department of Energy (DoE) in support of the Open Government Initiative to make energy data transparent and collaborative. The measured historical annual data set is used to estimate the parameters of the generalized Gaussian mixture model using the E-M algorithm. The E-M algorithm is coded in MATLAB and initialized using the K- means algorithm. A random number generator function generates statistically similar load profile scenarios. The random number generator function can be evaluated by taking the inverse of the CDF of the mixture model. The CDF of the mixture model in (12) is

$$F_Y(y|\Psi) = \int_{-\infty}^{y} \sum_{j=1}^{M} \pi_j \frac{\beta_j}{2s_j\Gamma\left(\frac{1}{\beta_j}\right)} \exp\left[-\frac{|t-\mu_j|^{\beta_j}}{s_j}\right] dt \tag{23}$$

A closed form solution of $\hat{y} = F_Y^{-1}(y|\Psi)$ does not exist and hence numerical techniques such as Newton-Raphson must be used to generate random samples from the fitted model. Figure 4 shows a hundred example scenarios of the load at bus 890 for one day. It is important to note that the load scenarios shown in Figure 4 also account for the PHEV charging. The scenarios for solar generation at bus 890 are generated using the Monte Carlo sampling of the fitted time series ARMA model. We assume a three-phase PV system at bus 890 with a peak power rating of 450 kW proportional to the peak active load. The voltage rating of the PV system is 4.16 kV. The PV system is oriented at an azimuth of 180 °(south-facing) and a tilt angle of 30 °. Since the IEEE-34 bus test feeder is based on an existing distribution system located in the state of Arizona (AZ), the hourly average TMY3 [10] data of

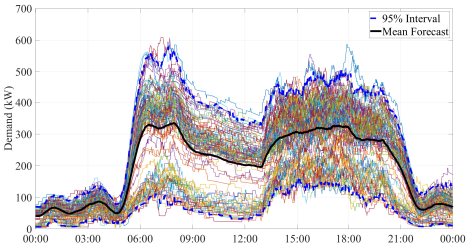

Figure 4. Load Scenarios at Bus 890 including PHEV charging Profiles

AZ is used to synthesize a high resolution (1-minute) irradiance profile. The solar output in 1-minute intervals is estimated using the PV system model in OpenDSS [13]. The high-resolution solar output data is used to fit the ARMA model. The fully realized ARMA model is used to generate solar forecasts. Figure 5 shows one hundred 1-minute ahead solar output scenarios for a typical spring day in AZ along with the mean forecast and 95% confidence interval. The parameters of the

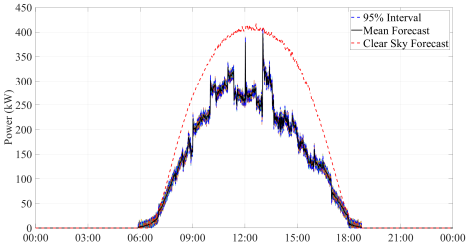

Figure 5. 1-minute ahead solar forecasts from ARMA model from Table 1

realized ARMA model are given in Table 1

Table 1. The Realized ARMA (p, q) Model

p	q	ϕ_i	θ_j
3	3	$\phi_1 = 0.376$ $\phi_2 = -0.3722$ $\phi_3 = 0.9848$	$\theta_1 = 0.6151$ $\theta_2 = 0.9845$ $\theta_3 = -0.005$

The generated scenarios of the input variables are used to calculate the Monte Carlo estimator of (7). This is done by taking the i.i.d sample $\{q_\gamma(t); \gamma = [1, 2, ...H,], t = [1, 2, ..., T]\}$. H is the total number of Monte Carlo runs and T is the time horizon. The time horizon considered in this work is one year. The mean of $(g(q_\gamma(t)))$ over the chosen sample is the estimate of $\mathbf{E}[h(Q_t)]$.

$$\hat{h}_\gamma\left(q_\gamma(t); t \in [1, T]\right) = \frac{1}{\gamma}\sum_{v=1}^{\gamma} h\left(q_v(t); t = \in [1, T]\right) \tag{24}$$

Assuming the expectation $\mathbf{E}[h(Q_t)]$ is finite, the weak law of large numbers implies for an arbitrarily small ϵ

$$\lim_{\gamma\to\infty}\left(\Pr\{\hat{h}_\gamma\left(q_\gamma(t); t \in [1, T]\right) - \mathbf{E}[h(Q_t)] \geq \epsilon\}\right) = 0 \tag{25}$$

Equation (25) implies that as γ gets large, the Monte Carlo estimator converges in probability to the true expectation. The i.i.d sample $\{q_\gamma(t); t = [1, 2, ..., T]\}$ for fixed γ is obtained by executing the power flow on the model of IEEE 34 bus test feeder in OpenDSS interfaced with MATLAB via COM. The capacitor-less D-STATCOM is placed at bus 890 of the test feeder. The power factor correction and voltage regulation programs are developed in MATLAB. The circuit is solved in OpenDSS with control actions suspended at first. This is done to sample the quantities of interest, i.e., bus voltage phasors and load reactive power for D-STATCOM initialization. Based on the retrieved values of the bus voltages and load, the programs populate the current injection sources that model D-STATCOM operation in power factor correction mode to compensate for the reactive power of the load. At the same time, the voltage regulation subroutine uses the reactive power mismatch equations to calculate the reactive power for maintaining bus voltage at a predefined set point. The modified circuit with D-STATCOM is solved again in OpenDSS with control actions enabled. Once the control queue clears, the program steps through the next solution.

The probability distributions of the capacity usage in voltage regulation mode $Q_{3\phi}^{vr}$ for different voltage set points considering the uncertainty in PHEV charging, commercial reactive demand and the solar generation is shown in Figure 6 The D-STATCOM adjusts its reactive

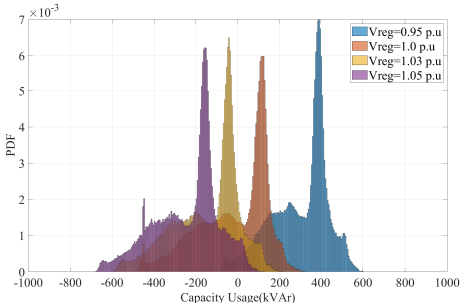

Figure 6. Capacity Usage in voltage regulation mode

output in accordance with (6). This ensures that the bus voltage is held nearly constant and equal to the voltage set point of the converter. Figure 6 suggests that for higher voltage set points the converter is more likely to absorb reactive power while for lower voltage set points the likelihood of injecting reactive power is more. The expected value of the capacity usage for power factor

correction is 121.95 kVAr, and for voltage regulation, the expected value of capacity usage is 474.62 kVAr. This is approximately four times higher than the power factor application. Furthermore, the standard deviation of $Q_{3\phi}^{pf}$ is 88.6 kVAr while the standard deviation of $Q_{3\phi}^{vr}$ is 162.95 kVAr. A higher standard deviation of $Q_{3\phi}^{vr}$ suggests greater uncertainty in its estimation. This could be because of the dual impact of intermittent solar generation and PHEV charging on the bus voltage. Figure 7 shows the capacity usage when the converter is operating in power factor correction mode in accordance with (2-5) It is clear that voltage regulation operation is more capacity intense than power factor correction. Interestingly, from Figure 7 the converter is more likely to inject power into the grid for power factor operation close to or at unity. This is consistent with the steady state power factor correction model (2-5).

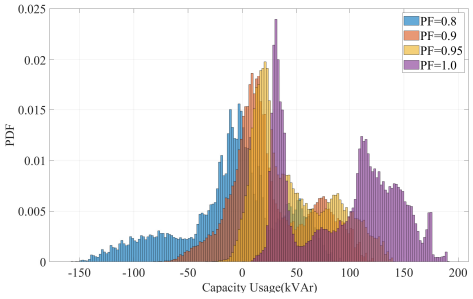

Figure 7. Capacity usage in power factor correction mode

An interesting application of the capacity usage results in Figure 6 and 7 is the determination of the energy loss due to the curtailment of the PV output when capacity sizing constraints on the converter are considered. The results in Figure 6 are valid for an unrestrained D-STATCOM. However, a restrained D-STATCOM will be limited in its ability to provide reactive power compensation. The limits placed on the converter capacity could either be due to the high manufacturing cost or the technology limitations that could preclude scaling the converter capacity. Since voltage regulation application utilizes more capacity, any limits on the converter capacity would primarily impede the converter's ability to regulate voltage. In order to maintain the bus voltage within acceptable limits, especially the upper limit of $1.05p.u$, additional measures such as curtailing the PV system's output must be put into effect. To observe the impact of the capacity reduction of the D-STATCOM on the energy loss due to the curtailment of PV output, we use the volt-watt control functionality in OpenDSS. It provides a flexible mechanism to regulate the active power output of a PV system based on a user-configured volt-watt control curve. For our application, we use a volt-watt curve that reduces the PV output whenever the bus voltage exceeds $1.05p.u$. If $\triangle g_{PV}^{i}(\omega)$ is the curtailed PV power at bus i for scenario ω, the energy loss over the planning horizon is

$$E_{loss}(\omega) = \int_0^T \triangle g_{PV}^{i}(\omega) dt \tag{26}$$

$E_{loss}(\omega)$ is a random variable and we are interested in the expectation $\mathbf{E}[E_{loss}(\omega)]$ as a function of the capacity reduction of the D-STATCOM. Figure 9 shows the cdf plots of energy loss of a 450 kW PV system at bus 890. The converter is programmed to maintain the bus voltage at $1p.u$ and the capacity is reduced in steps of 10% from the baseline capacity of $+/-$ 900 kVAr. It can be inferred from Figure 8 that the probability of energy loss increases with the reduction in converter capacity. For capacity reductions up to 20% there is roughly 70% probability of incurring an annual energy loss of 5% or less. The probability of energy loss however dramatically increases as the converter capacity is further reduced. Figure 9 plots the expectation

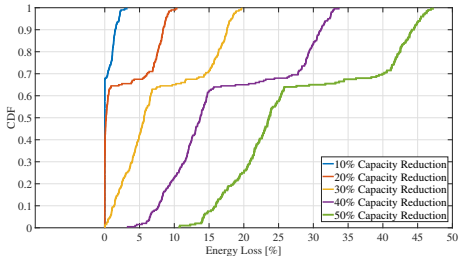

Figure 8. CDF plots of loss of energy $E_{loss}(\omega)$

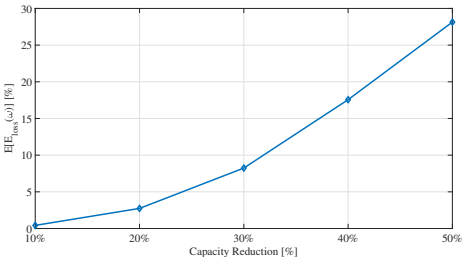

Figure 9. Expected value of Annual Energy loss of a 450 kW PV System

$\mathbf{E}[E_{loss}(\omega)]$ as a function of the capacity reduction of the proposed converter. A 50% reduction in the converter capacity would result in an annual energy loss of nearly 30% of the value if the converter was operating at full capacity with a voltage setpoint of $1.0p.u$. On the other hand a capacity reduction up to 20% could be acceptable as the energy loss is less than 5%.

5. Acknowledgements

This publication was made possible by NPRP grant # 13S-0213-200357 from the Qatar National Research

Fund (a member of Qatar Foundation). The statements made herein are solely the responsibility of the authors.

6. Conclusions

In this paper, we study the capacity usage of the proposed capacitor-less D-STATCOM in a distribution system, considering the uncertainties in PHEV charging, system demand, and solar generation. Two different modes of operation of the converter are presented. The power factor correction operation is modeled as an ideal current source shunt connected to the load. The voltage regulation mode of operation is modeled based on the reactive power mismatch equations between the converter and the load bus.

To assess the uncertainty in the capacity usage, Monte Carlo simulations are designed with inputs sampled from their underlying distributions. Various scenario generation algorithms consistent with the physics and based on real-world measured data are presented to sample the input parameters. Based on the results of the Monte Carlo runs, it is concluded that voltage regulation operation utilizes more capacity than power factor correction and is characterized by a higher variance. Furthermore, restraining the capacity of the converter increases the energy loss due to the curtailment of the PV output. More precisely, the expected value of the loss of energy shares a nonlinear relationship with the capacity reduction of the converter. The energy loss increases with the progressive decrease in the capacity of the converter.

The methodology and the results presented in this paper are important and can be used as a tool by the manufacturers to improve the design and functionalities of the power electronic converters for use in distribution systems. In the future, we plan on extending this work to include more complex distribution systems with more components, such as the IEEE-123 bus feeder and the 8500 node test feeder.

References

[1] R. B. Faruque, M. F. Scudder, and S. Ula, "Real-World Implementation of Advanced PV Curtailment and Reactive Power Control Using Non-Smart PV Inverter: A Case Study," *IEEE Power and Energy Society General Meeting*, vol. 2020-August, 8 2020.

[2] W. Rohouma, R. S. Balog, A. A. Peerzada, and M. M. Begovic, "D-STATCOM for harmonic mitigation in low voltage distribution network with high penetration of nonlinear loads," *Renewable Energy*, 2020.

[3] W. Rohouma, M. Metry, R. S. Balog, A. A. Peerzada, M. M. Begovic, and D. Zhou, "Analysis of the Capacitor-Less D-STATCOM for Voltage Profile Improvement in Distribution Network With High PV Penetration," *IEEE Open Journal of Power Electronics*, vol. 3, pp. 255–270, 2022.

[4] W. Rohouma, M. Metry, R. S. Balog, A. A. Peerzada, and M. M. Begovic, "Adaptive Model Predictive Controller to Reduce Switching Losses for a Capacitor-Less D-STATCOM," *IEEE Open Journal of Power Electronics*, vol. 1, pp. 300–311, 8 2020.

[5] O. Hafez and K. Bhattacharya, "Queuing analysis based PEV load modeling considering battery charging behavior and their impact on distribution system operation," *IEEE Transactions on Smart Grid*, 2018.

[6] M. Alizadeh, A. Scaglione, J. Davies, and K. S. Kurani, "A scalable stochastic model for the electricity demand of electric and plug-in hybrid vehicles," *IEEE Transactions on Smart Grid*, 2014.

[7] S. Bae and A. Kwasinski, "Spatial and temporal model of electric vehicle charging demand," *IEEE Transactions on Smart Grid*, 2012.

[8] R. Singh, B. C. Pal, and R. A. Jabr, "Statistical representation of distribution system loads using Gaussian mixture model," *IEEE Transactions on Power Systems*, 2010.

[9] A. Peerzada, M. Begovic, and D. Ostojic, "On the Environmental and Economic Impact of Utility-scale Renewable Energy Deployment,"

[10] S. Wilcox, "National Solar Radiation Database 1991–2010 Update: User's Manual ," *Nrel/Tp-5500-54824*, 2012.

[11] B. Singh and D. Pozo, "A Guide to Solar Power Forecasting using ARMA Models," *Proceedings of 2019 IEEE PES Innovative Smart Grid Technologies Europe, ISGT-Europe 2019*, 9 2018.

[12] K. P. Schneider, B. A. Mather, B. C. Pal, C. W. Ten, G. J. Shirek, H. Zhu, J. C. Fuller, J. L. Pereira, L. F. Ochoa, L. R. De Araujo, R. C. Dugan, S. Matthias, S. Paudyal, T. E. McDermott, and W. Kersting, "Analytic Considerations and Design Basis for the IEEE Distribution Test Feeders," *IEEE Transactions on Power Systems*, 2018.

[13] R. C. Dugan, "The Open Distribution System Simulator (OpenDSS)," tech. rep., 2012.

[14] P. A. Lewis and G. S. Shedler, "SIMULATION OF NONHOMOGENEOUS POISSON PROCESSES BY THINNING.," *Naval research logistics quarterly*, 1979.

[15] Y. Chen, "Thinning Algorithms for Simulating Point Processes," tech. rep., 2016.

[16] C. M. Affonso and M. Kezunovic, "Probabilistic assessment of electric vehicle charging demand impact on residential distribution transformer aging," in *2018 International Conference on Probabilistic Methods Applied to Power Systems, PMAPS 2018 - Proceedings*, 2018.

[17] N. Sammaknejad, Y. Zhao, and B. Huang, "A review of the Expectation Maximization algorithm in data-driven process identification," 2019.

[18] D. A. Dickey and W. A. Fuller, "Distribution of the Estimators for Autoregressive Time Series With a Unit Root," *Journal of the American Statistical Association*, vol. 74, p. 427, 6 1979.

[19] "System Identification Toolbox Documentation."

[20] Office of Energy Efficiency & Renewable Energy, "Commercial and Residential Hourly Load Profiles for all TMY3 Locations in the United States - Datasets - OpenEI Datasets," 2015.